

A Tesla pulse transformer for spiral water pulse forming line charging

J.-L. LIU,^{1,2} T.-W. ZHAN,² J. ZHANG,² Z.-X. LIU,² J.-H. FENG,² T. SHU,² J.-D. ZHANG,² AND X.-X. WANG¹

¹Department of Electrical Engineering, Tsinghua University, Beijing, China

²College of Photoelectrical Engineering and Science, National University of Defense Technology, Changsha, China

(RECEIVED 4 November 2006; ACCEPTED 31 January 2007)

Abstract

A high voltage pulse Tesla transformer with a coupling coefficient of 0.75 was designed and experimentally investigated. The transformer was employed to charge a spiral water pulse forming line (PFL) in a high current electron beam accelerator, and was featured by its compactness, stability, and reliability. When the primary input voltage is 55 kV, the transformer can charge the PFL to 720 kV with an energy conversion efficiency of 36%. The formulas for calculating the primary and secondary inductances of the transformer were deduced, with which the main parameters of the transformer were calculated theoretically. The distributions for electrical and magnetic fields in the transformer were obtained by the simulations of calculation. In addition, the process of an accelerator of the transformer charging a spiral PFL was simulated through the Pspice software to get the waveform of charging voltage, the diode voltage, and diode current of accelerator. The theoretical and simulated results agree with the experimental results.

Keywords: Electron beam accelerator; Pulsed power; Spiral pulse forming line; Tesla transformer

1. INTRODUCTION

High current electron beam accelerators are widely used in both civilian and military fields. Long pulse (Friedman *et al.*, 1988; Korovin *et al.*, 2001) and high repetition (Kitsanov *et al.*, 2002; Rukin *et al.*, 1999; Lyubutin *et al.*, 1999) are currently two very important development trends for an accelerator. Using spiral technique to modify the coaxial PFL (Yang *et al.*, 2005) is an effective method to achieve long pulse at a given length of PFL. In the long pulse accelerators based on spiral PFL, air-core transformers (Rohwein, 1979; Liu *et al.*, 2003, 2006), or Tesla transformers (Korovin, 1996) with ferromagnetic core were employed widely.

There are two basic types of high-voltage air-core pulse transformers (Sarjeant *et al.*, 1983). The first is the spiral-strip type (Fig. 1a). The second is the single-layer helical wire transformer (Fig. 1b). These transformers differ from each other primarily in the configuration of the secondary windings, which accounts for a significant difference in their resistance to insulation failure from fast pulse. The

primary windings for either type, whether single or multiple turn, may be designed in a variety of ways, without affecting the electrical breakdown characteristics of the transformers. For reason of high voltage isolation, the low voltage primary winding is typically placed outside and the secondary winding is led out through the center of the assembly.

Two problems are common to both types of transformers. The first problem is electrical breakdown turn to turn in the helical transformer or between windings in the spiral strip transformer. The second problem is energy loss from eddy currents induced in the voltage grading devices and structural components in the transformers. Both types of transformers are well suited for single frequency applications, such as pulse charging high voltage PFL (Rohwein, 1979; Liu *et al.*, 2006). However, there are no ferromagnetic cores in the transformers; magnetic saturation will not be formed in the case of intense current flowing primary winding. The transformers can charge high voltage PFL only when the transformer involves the primary current levels that are over a megampere. Furthermore, the air-core pulse transformer has constructing compact, light weight, and wide bandwidth.

At present, another type of transformer that is widely applied in high power pulse power field is the pulsed

Address correspondence and reprint requests to Jinliang Liu, College of Photoelectrical Engineering and Science, National University of Defense Technology, Changsha, 410073, China. E-mail: ljle333@yahoo.com

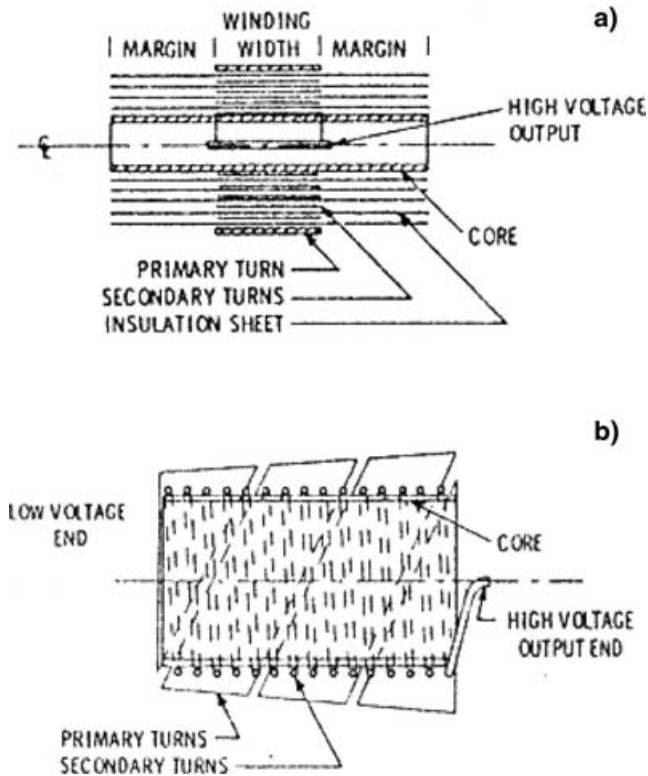


Fig. 1. Schematic of the high power air-core transformer.

transformer with ferromagnetic core or bars. It can be employed to provide repetitive regime for high voltage generators and charging high voltage oil-pulse-forming transmission lines of an accelerator. For this purpose, the Institute of High Current Electronics proposed the use of a Tesla transformer with high coupling coefficient (Kitsanov *et al.*, 2002). Combining a Tesla transformer with a forming line allowed producing compact, reliable repetitively pulsed high voltage generators (Korovin & Rostov, 1996). The geometry of this coaxial system is presented in Figure 2a. Its output voltage to charging oil-pulse-forming line is over 1 MV at 100 ps, when the input voltage of primary winding of a Tesla transformer is 400–700 V. The coupling coefficient of the transformer is over 0.9.

Spiral-strip transformers with a partial magnetic core is also researched and applied in the pulse power field (Rohwein *et al.*, 1981; Liu *et al.*, 2006). The high voltage pulse forming network (PFN) pulse transformer system (Rohwein *et al.*, 1981) was designed at the Sandia National Laboratories with a $10\times$ voltage setup and a $0.5\ \Omega$, $2\ \mu\text{s}$ PFN. The maximum output voltage for the transformer was 200 kV with a $50\ \Omega$ load. The cross-section of this type of transformer with compact and lightweight is presented in Figure 2b.

Although the air-core transformer have the advantages of a simple structure, small volume, and light weightiness, it is not suitable for high repetition applications because of its low coupling coefficient, low energy conversion efficiency, and difficulty in heat dispersion. Therefore, the Tesla

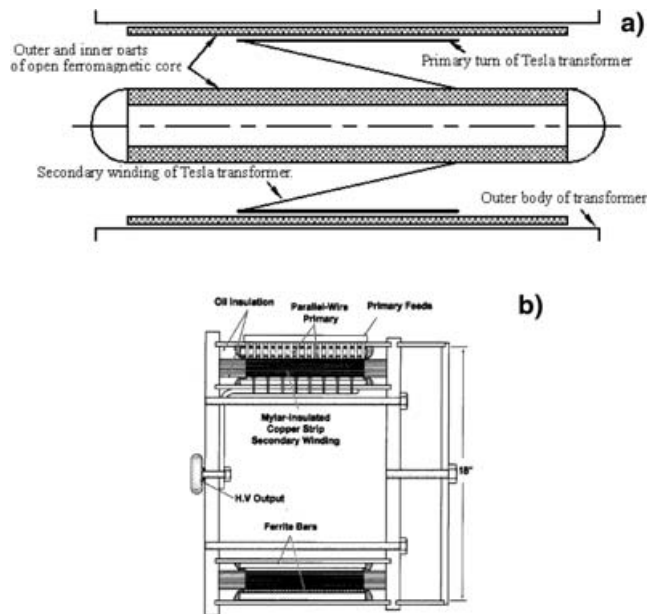


Fig. 2. High power transformers with magnetic core.

transformer with open magnetic core, which can operate repetitively due to its high coupling coefficient, and high-energy conversion efficiency, is often used in the repetitive accelerator based on the oil-PFL. However, the conventional Tesla transformer can not be employed to charge water-PFL due to its long charging time, which may result in energy loss in the charging process, or water breakdown. Therefore, in this paper, a high voltage pulse Tesla transformer for charging water-PFL in a long pulse accelerator was developed. The structure of the transformer was described and its main parameters were calculated. Moreover, simulations were conducted to investigate its electric characteristics. Experimental results confirm the design idea and the simulation results, showing that the transformer can charge the water-PFL in the long pulse accelerator to a high voltage of over 700 kV within about $3.5\ \mu\text{s}$, with the energy conversion efficiency of about 36%.

2. STRUCTURE OF THE TRANSFORMER

The high voltage pulse Tesla transformer is schematically shown in Figure 3. It consists of primary windings, secondary windings, inside and outside magnetic cores, voltage input, high voltage output, and supporting case. The primary winding is made from a copper strip with a width of 30 cm, thickness of 0.5 mm, and turns of 2.25.7 layers of polyester films with a width of 40 cm and thickness of 0.1 mm, to provide the turn-to-turn insulation. The voltage of the primary windings is introduced through the voltage input. The secondary windings are made from a 3 mm copper line, which is wound along a spiral groove on a tapered nylon stick, the distance between turns is 2 mm, and is fastened with insulation glue. The outside magnetic core is a hollow cylinder made by the strip tinny-steel

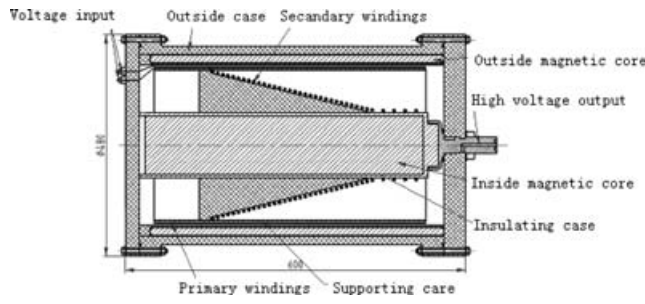


Fig. 3. Cross section of Tesla transformer with magnetic core.

piece of thickness of 0.35 mm, tightly located between the primary windings and the supporting case. The inside magnetic core is a solid cylinder also made by the strip tinny-steel piece of thickness of 0.35 mm, embedded inside the nylon stick coaxially. The supporting case, made from fiberglass, houses the components of the transformer, fastens the primary winding to avoid distortions and displacements, resulting from electromotive force while the transformer is operating. The transformer oil is filled in the supporting case to ensure electric insulation inside the transformer (before the oil was filled, all components inside the transformer had been degassed). In the accelerator based on water-PFL, the transformer was connected to the outer tube of the PFL through a flange of the supporting case, and its high voltage output was connected to the inner conductor of the PFL to perform charging.

3. THEORETICAL CALCULATION AND CIRCUIT SIMULATION

3.1. Theoretical calculation of main parameters of the transformer

In order to obtain the electric characteristic of the transformer and the voltage and current wave of the diode of the accelerator theoretically, it is necessary to calculate the primary and secondary inductances, and the coupling coefficient of the transformer. The cross-section of the magnetic cores of the transformer is shown in Figure 4.

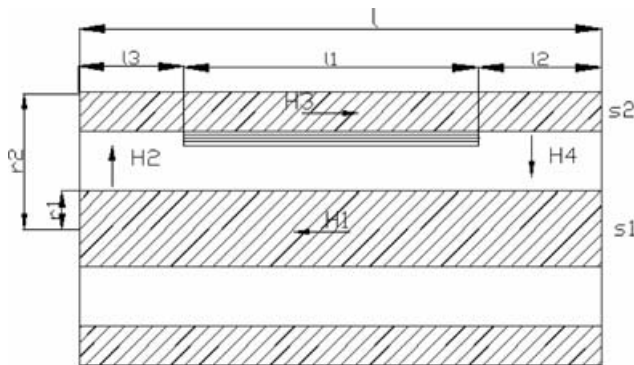


Fig. 4. Cross section of magnetic cores in the transformer.

In the case where the length of the magnetic core is much greater than the outer radius of the secondary windings (over four times larger usually) and the couple coefficient is relatively large (greater than 0.7 usually), the magnetized inductance is mainly determined by the properties of the magnetic cores. Therefore, the magnetic flux leakage could be omitted. Assuming r_1 is the radius of the inside magnetic core, r_2 is the outer radius of the outside magnetic core, l_1 is the width of the windings, l_2 and l_3 are the widths of two margins on each side of the windings, S_1 and S_2 are the cross-section area of the inside and outside magnetic cores, H_1 , H_2 , H_3 , and H_4 are the magnetic field intensity of the corresponding parts indicated in Figure 4.

When ignoring the margining effects of the magnetic field, the energy of the magnetic field is

$$\frac{1}{2}L_{\mu}I^2 = \int \frac{1}{2}\vec{B} \cdot \vec{H} dV, \quad (1)$$

where V is the volume of the magnetic field. Hence the magnetized inductance L_{μ} is represented by

$$\begin{aligned} L_{\mu} &= \frac{1}{I^2} \int \vec{B} \cdot \vec{H} dV \\ &= \mu H_1^2 S_1 l + \mu H_3^2 S_2 l + 2\pi\mu_0 l_3 \int_{r_1}^{r_2} H_2^2 r dr \\ &\quad + 2\pi\mu_0 l_2 \int_{r_1}^{r_2} H_4^2 r dr \end{aligned} \quad (2)$$

Without regard to the eddy effect and the non-uniform distribution of the magnetic field on the cross-section, according to the equation of $\vec{B} \cdot d\vec{s} = 0$, the following equations are inferred:

$$\oint \vec{B} \cdot d\vec{s} = \mu H_1 S_1 - 2\pi r \mu_0 l_3 H_2(r) = 0, \quad (3)$$

$$\oint \vec{B} \cdot d\vec{s} = \mu H_1 S_1 - 2\pi r \mu_0 l_2 H_4(r) = 0. \quad (4)$$

From the magnetic flux conservation of the inside and outside magnetic cores, i.e., $\Phi = H_1 S_1 = H_3 S_2$ and the magnetic field intensity is given by:

$$H_2 = \frac{\mu_r S_1 H_1}{2\pi r l_3}, \quad (5)$$

$$H_3 = \frac{S_1}{S_3} H_1 = \frac{1}{\alpha} H_1, \quad (6)$$

$$H_4 = \frac{\mu_r S_1 H_1}{2\pi r l_2}. \quad (7)$$

According to $\oint \vec{H} \cdot d\vec{l} = N_1 I_1$, the relationship between

current and magnetic field is as follows

$$H_1 l + \int_{r_1}^{r_2} H_2 dr + H_3 l + \int_{r_1}^{r_2} H_4 dr = 0. \quad (8)$$

Substituting (5), (6), and (7) into (8), we obtain

$$H_1 = \frac{2\pi N_1 I_1 \alpha l_2 l_3}{2\pi l \alpha l_2 l_3 + 2\pi l l_2 l_3 + \mu_r S_1 \alpha l_2 \ln \beta + \mu_r S_1 \alpha l_3 \ln \beta}, \quad (9)$$

where

$$\beta = \frac{r_2}{r_1}.$$

Substituting (5), (6), (7), and (9) into (2) gives the following

$$L_\mu = \frac{H_1^2 (2\mu S_1 l \alpha^2 \pi l_2 l_3 + 2\mu S_2 l \pi l_2 l_3 + \mu_0 \ln \beta \mu_r^2 S_1^2 \alpha^2 l_2 + \mu_0 \ln \beta \mu_r^2 S_2^2 \alpha l_3)}{\alpha^2 \pi l_2 l_3}. \quad (10)$$

Assuming H_p is the magnetic field intensity produced by the primary winding current I_p , and H_s is the reverse magnetic field intensity produced by the secondary winding current I_s , the leakage inductance is defined by the following relationship

$$L_s = \frac{\mu}{l_s^2} \int (H_p - H_s)^2 dV. \quad (11)$$

The method for calculating the magnetic field intensity produced by the secondary windings is the same as that for the primary windings described above. Assuming H'_1 , H'_2 , H'_3 , and H'_4 are the magnetic field intensity produced by the secondary windings at corresponding parts indicated in Figure 4, therefore, leakage inductance is as follows

$$L_s = \mu S_1 l (H_1 - H'_1)^2 + \mu (H_3 - H'_3)^2 + 2\pi \mu_0 l_3 [(H_2 r)^2 + (H'_2 r)^2 - 2(H_2 r)(H'_2 r)] + 2\pi \mu_0 l_2 [(H_4 r)^2 + (H'_4 r)^2 - 2(H_4 r)(H'_4 r)]. \quad (12)$$

According to the experiential formula (Koroven, 1996), the couple coefficient is defined by

$$k^2 = 1 - \frac{2}{3} \frac{r_2^2}{l_k (l_T - l_k)} F(\beta), \quad (13)$$

where $F(\beta) = ((\beta - 1)(2\beta + 1))/\beta^2$, l_T and l_k are the length of the magnetic core and the windings, respectively. Therefore, the inductances of primary and secondary windings are written as follows

$$L_1 = L_\mu + L_s \quad (14)$$

Table 1. Comparison between calculated results and experimental results

	Calculated results (μH)	Experimental results (μH)	Relative error
Primary windings inductance	2.21	2.26	2.2%
Secondary windings inductance	1522.92	1465.48	3.9%
Coupling coefficient	0.76	0.75	1.3%

$$L_2 = \left(\frac{N_2}{N_1}\right)^2 L_\mu. \quad (15)$$

As for the designed transformer, $N_1 = 2.25$, $N_2 = 60$, $r_1 = 0.04$ m, $r_2 = 0.15$ m, $l_1 = 0.3$ m, $l_2 = 0.055$ m, $l_3 = 0.11$ m, $l_T = 0.55$ m, $\mu_r = 640$. With the above formula, the following calculated results were obtained and shown in Table 1, and their corresponding experimental results are also given in Table 1.

As indicated in Table 1, the calculated results agree well with the experimental results. Therefore, the method described above can be used to calculate the main parameters of the transformer.

3.2. Simulation of electromagnetic field of the transformer

In the above theoretical calculations for obtaining the primary and secondary inductances of the transformer, we suppose that the eddy current and the none uniform of the magnetic field distribution on the cross-sections of the magnetic cores can be neglected, so the energy of the magnetic field is totally concentrated in the inner and outer magnetic cores, as well as the annular gap between them. To verify the reasonability of the assumption, electromagnetic field analysis on the transformer was carried out by employing an ANSYS software for calculating the electromagnetic field, which is based on the finite element method (FEM), and capable of solving the capacitance, inductance, and electromagnetic field distribution for a model. Due to the propagating velocity for the electromagnetic field, are the light velocity and the time scale for the input voltage of the transformer in microsecond, so that the distributions for the electrical field and the magnetic field in the transformer can be regarded as a stationary field in the time period of the transformer being input. Moreover, the structure of the transformer is coaxial, so a two-dimensionally axial-symmetric model can be used in simulations, which is also helpful to reduce the calculation scale.

First, the two-dimensional stationary magnetic field distributions in the transformer were simulated. Figure 5 shows

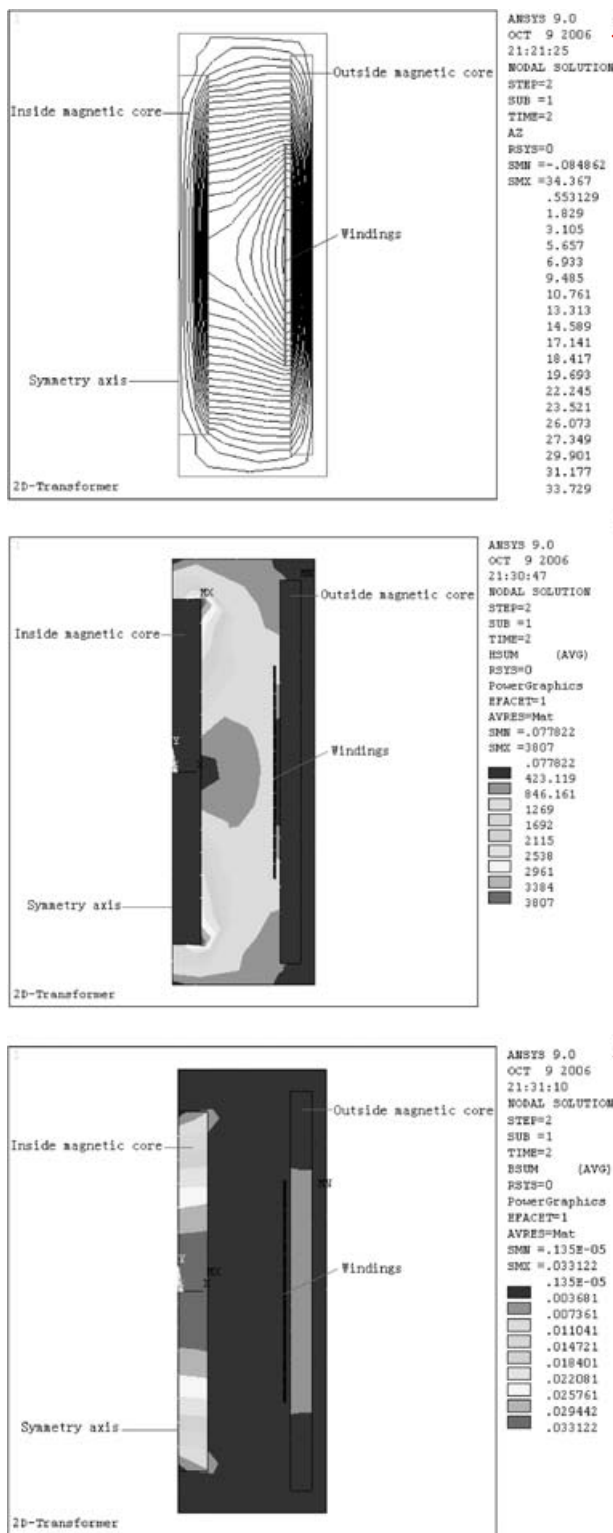


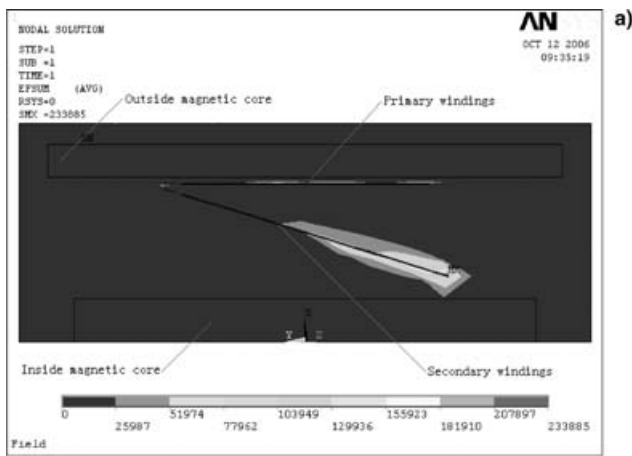
Fig. 5. Stationary magnetic field distributions in the transformer.

the distributions of the magnetic flux line, magnetic field intensity, and magnetic induction intensity in the transformer, respectively. Figure 5a suggests that the magnetic flux lines produced by the current flowing in the primary

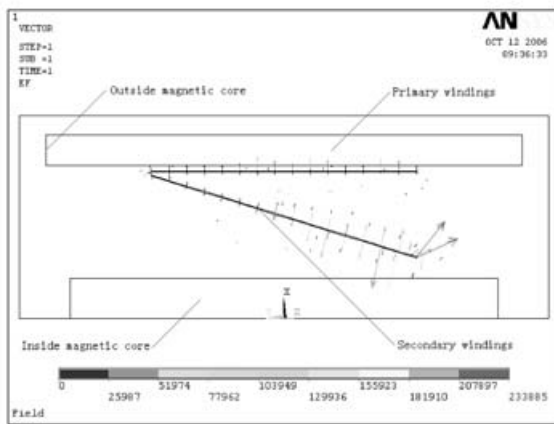
copper strip are mainly located in the inner and outer magnetic cores, as well as the gap between them; since the magnetic energy is the volume integral of the production of magnetic field intensity, and magnetic induction intensity, so the magnetic field intensity distribution shown in Figure 5b indicates that the magnetic energy is also mainly located in the inner and outer magnetic cores, as well as the gap between them. In the transformer with such a coaxial structure, the cross-section area for the inner magnetic core is smaller than that of the outer magnetic core. Therefore, according to the law of magnetic flux conservation, we can conclude that the magnetic induction intensity in the inner core is bigger than that of the outer core, which is clearly demonstrated in Figure 5c. Since the magnetic field intensity is defined as $H = B/\mu_r\mu_0$, and the magnetic field intensity in air is 10 times smaller than that in the magnetic cores, and the permeability μ_r in the magnetic cores is 10^4-10^5 times bigger than that in air, so the magnetic induction intensity in air is much bigger than that in magnetic core, which is also shown in Figure 5c. Through the above simulations on the magnetic field distribution, we can see that the secondary winding lying between the inner core and the outer core will get a very good magnetic induction, which is the main principle for this kind of transformer. In addition, according to the structure of the transformer given in Figure 3 and its operation principle, we also simulated the electric field distribution in the transformer. In our simulations, a primary voltage was exerted uniformly on the primary copper strip, and a corresponding secondary voltage was exerted on the secondary winding with a linear distribution from the ground end to the high voltage end. The obtained contour and vector distributions for the electric field intensity are shown in Figure 6. Figure 6a suggests that the maximum electrical field intensity is located around the high voltage end of the secondary winding. Figure 6b indicates that the directions of the electrical field intensity are mostly vertical to the plane where the secondary winding is located in. So, when designing the transformer, the insulation of the high voltage end and the insulation between adjacent circles of the secondary winding should be paid more attentions. Through the electrical field simulations, the strength of electrical field and its distribution were obtained, which provides an important instruction for the insulation designing of the transformer.

3.3. Circuitous simulation of an accelerator of the transformer charging a spiral PFL

For the electronic accelerator based on a helical line (Fig. 9), Pspice circuit analysis was used to model the accelerator. Figure 7 shows schematically the circuit model. The primary circuit includes an energy storage capacitor C2, parasitical resistance R34, inductance L12 of the primary circuit, a triggered gas switch U1, and the primary inductance of the transformer. The gap spark switches in the accelerator are modeled and indicated by Gap_{main} in the circuit. T indicated



a)



b)

Fig. 6. Stationary electric field distributions in the transformer.

the transmission line to simulate the helical line. The load of transmission line is modeled by the resistant value that matches the impedance of the helical line, and load is indicated by R37 in the circuit. In the circuit, the transformer is indicated by X_{form1} with the primary inductance of 2.26 μ H, the secondary inductance of 1465.48 μ H, and the coupling coefficient of 0.75, and the resistances of resistant dividers to measure the voltage of charging helical line, and the current of field-emission diode are indicated by R35 and R36, respectively. The whole circuit is connected with components built in Pspice component storage or modeled by the authors according to the performance of the device. Parameters for all components in the circuit are valued according to the practical circuit or theoretical

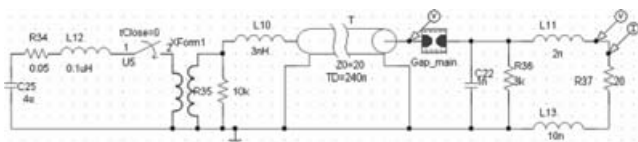
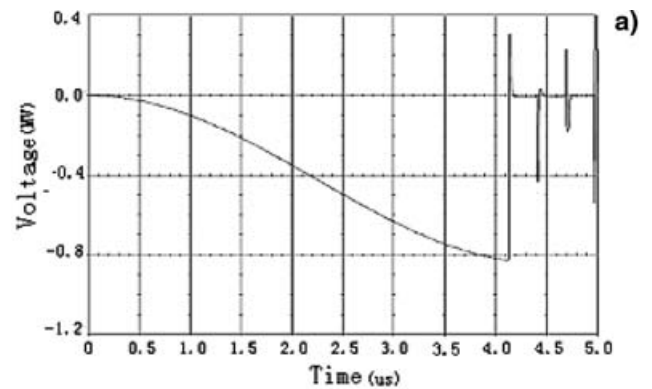
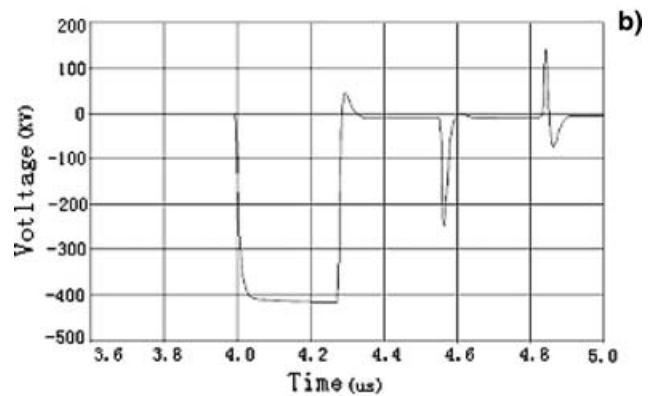


Fig. 7. Circuit schematic for simulating the electronic accelerator based on helical line.

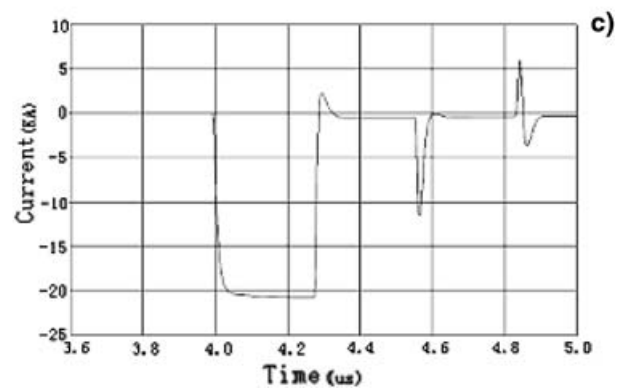
calculation given in Figure 7. The circuit was simulated through the Pspice software. In simulations, the energy storage capacitor (C25), initially charged at 55 kV, discharges to the primary winding of the transformer as the triggered switch closes. The obtained waveform of the charging voltage waveform of the helical line is shown in Figure 8a. According to Figure 8, the waveform has a peak voltage of 810 kV and a time of about 4 μ s for reaching the peak in its first pulse. Therefore, the transformer is suitable for charging a water helical line. The Pspice simulation results of voltage, current in the load are shows Figures 8b and 8c, respectively. As can be seen from Figures 8b and 8c, the voltage of the load is about 420 kV, and the current of the load is 22 kA, and the pulse duration is about 240 ns.



a)



b)



c)

Fig. 8. Simulation result of voltage and current signals.

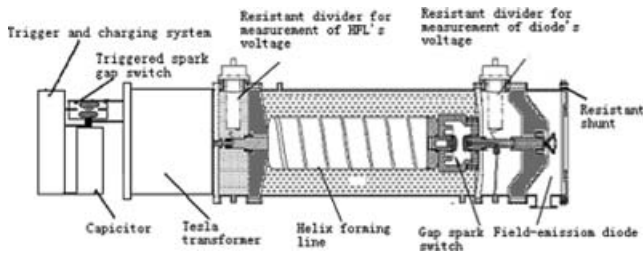


Fig. 9. Diagram of the electron accelerator based on a spiral water PFL.

4. EXPERIMENTAL RESULTS

The designed Tesla transformer was applied to a high current electron beam accelerator based on spiral water-PFL. The structure of the accelerator is shown in Figure 9. It consists of charging and triggering systems, an energy-storage capacitor, a triggered gas switch, the designed transformer, a spiral water-PFL, a self-breaking gas switch, a vacuum diode, and some related measuring systems. The operating process of the accelerator is as follows: while the charging voltage of the energy-storage capacitor reaches a certain value, the triggered gas switch is triggered and closed, then the energy-storage capacitor is discharged into the primary winding of the transformer. Consequently, the transformer starts to charge the PFL. Once the charging voltage of the PFL reaches the breakdown value of the self-breaking gas switch, the PFL is discharged into the vacuum diode, and the high current electron beam will be generated readily. As for deionized water filled in the PFL, its breakdown voltage for the negative pulses is about two times larger than that for positive pulses (Fenneman & Gripshover, 1980), so the self-breaking gas switch must be adjusted so that it will breakdown at the peak of the first negative pulse, otherwise, the water breakdown will happen as a positive pulse exerting on the PFL.

In experiments, the energy-storage capacitor was initially charged at 55 kV, and the charging waveform of the transformer to the PFL is shown in Figure 10. According to

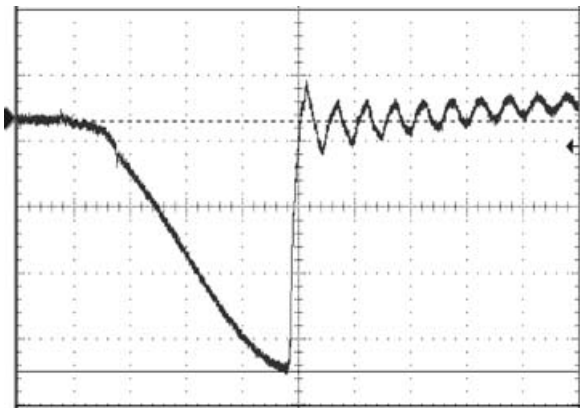


Fig. 10. Charging voltage waveform on spiral water PFL by Tesla transformer (Voltage: 200 kV/div Sweep = 1 μs).

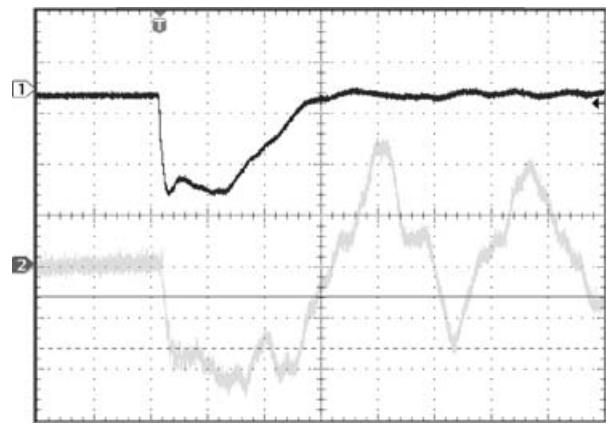


Fig. 11. Voltage (CH1) and current (CH2) waveform on the vacuum diode (Voltage: 200 kV/div Current: 10 kA/div Sweep = 200 ns).

Figure 10, the peak charging voltage is about 720 kV and the charging time is about 4 μs. The energy conversion efficiency of a transformer charging to a PFL equals the ratio between the energy stored in the energy-storage capacity and that in PFL, so the energy conversion efficiency of the designed transformer is 36%. The waveforms of the diode voltage and current of the accelerator are shown in Figure 11. The diode voltage is 400 kV, current is 18 kA, and pulse duration is over 200 ns, which agree with simulated results.

5. CONCLUSIONS

A high voltage pulse Tesla transformer was designed and experimentally investigated. The transformer was applied to a high current electron beam accelerator for charging spiral water-PFL, and was featured by its compactness, stability, and reliability. With the transformer, the accelerator produced an electron beam with a voltage of about 400 kV, current of 18 kA, and pulse duration of over 200 ns. To increase the coupling coefficient of the designed transformer and to operate the intense current electron beam accelerator at repeating frequencies, more research is needed.

ACKNOWLEDGMENTS

The author wishes to thank B.L. Qian, H.Y. Yang, and C.L. Liu for their encouragement and valuable suggestions. The assistance of X. Zhou, L. Luo, Q.M. Tan, and L.Y. Xu in the assembly and testing of the transformer is also gratefully acknowledged. This work was supported by the Chinese National Natural Science Foundation under grant 10675 168.

REFERENCES

FENNEMAN, D.B. & GRIPSHOVER, R.J. (1980). Experiments on electrical breakdown in water in the microsecond regime. *IEEE Trans. Plasma Sci.* **8**, 209–213.

- FRIEDMAN, S., LIMPAECHER, R. & SIRCHIS, M. (1988). Compact Energy Storage using a Modified-Spiral PFL. *IEEE Trans. Plasma Sci.* **20**–22, 367–372.
- KITSANOV, S.A., KLIMOV, A.I. & KOROVIN, S.D. (2002). A vircator with electron beam premodulation based on high-current repetitively pulsed accelerator. *IEEE Trans. Plasma Sci.* **30**, 274–285.
- KOROVIN, S.D. (1996). Tesla transformer for repetitive rate accelerator with high power. *Guowai Heshiyan Jishu* **19**, 1–23.
- KOROVIN, S.D. & ROSTOV, V.V. (1996). High-current nanosecond pulse-periodic electron accelerators utilizing a Tesla transformer. *Russian Phys. J.* **39**, 456–463.
- KOROVIN, S.D., GUBANOV, V.P., GUNIN, A.V., PEGEL, I.V. & STEPCHENKO, A.S. (2001). Repetitive nanosecond high-voltage generator based on spiral forming line. *Pulsed Power Plasma Sci.* **2**, 1249–1251.
- LIU, J.L., ZHANG, J.D. & LI, Y.Z. (2003). High voltage pulse transformer for PFL charging. *High Power Laser Part. Beams* **15**, 394–396.
- LIU, J.L., LI, C.L., ZHANG, J.D., LI, S.Z. & WANG, X.X. (2003). A spiral transformer type electron-beam accelerator. *Laser Part. Beams* **24**, 355–358.
- LIU, J.L., SHI-ZHONG, L. & JIAN-HUA, Y. (2006). Primary research on high power strip pulse transformer with magnetic core. *High Power Laser Part. Beams* **18**, 1736–1740.
- LUYBUTIN, S.K., RUKIN, S.N., SHARYPOV, K.A., SHPAK, V.G., SHUNAILOV, S.A., SLOVIKOVSKY, B.G., ULMASKULOV, M.R., YALANDIN, M.I., KOROVIN, S.D. & ROSTOV, V.V. (1999). Nanosecond microwave generator based on the relativistic 38 GHz backward wave oscillator and all-solid-state pulsed power modulator [A]. *IEEE Trans. Plasma Sci.* **30**, 1220–1225.
- ROHWEIN, G.J. (1979). A 3 MV Transformer for PFL Pulse Charging. *IEEE Trans. Nucl. Sci.* **26**, 4211–4213.
- ROHWEIN, G.J., LAWSON, R.N. & CLARK, M.S. (1981). A Compact 200 kV Pulse Transformer System. *IEEE Trans. Plasma Sci.* **30**, 968–970.
- RUKIN, S.N., MESYATS, G.A., DARZNEK, S.A., LYUBUTIN, S.K., PONOMAREV, A.V., SLOVIKOVSKY, B.G., TIMOSHENKOV, S.P., BUSHLYAKOV, A.Z. & TSIRANOV, S.N. (1999). SOS-based pulsed power: Development and applications. *IEEE Trans. Plasma Sci.* **30**, 153–156.
- SARJEANT, W.G. & ROHWEIN, G.J. (1983). A review of repetitive pulse power component technology. 4th IEEE International Pulsed Power Conf. New Mexico, USA., 303–308.
- YANG, J.H., ZHONG, H.H., TING, S. & ZHANG, J.D. (2005). Water-dielectric Blumlein type of PFL with line. *High Power Laser Part. Beams* **17**, 1191–1194.